Variation of growth morphology with chemical composition of terraces: Ag on a twofold surface of a decagonal Al-Cu-Co quasicrystal

T. Duguet,[1,2,3] B. Ünal,[1,2,*] Y. Han,[4,5] J. W. Evans,[4,5] J. Ledieu,[3] C. J. Jenks,[1,2] J. M. Dubois,[3] V. Fournée,[3] and P. A. Thiel[1,2]

[1]*Ames Laboratory, U.S. Department of Energy, Department of Chemistry, Iowa State University, Ames, Iowa 50011, USA*

[2]*Department of Materials Sciences & Engineering, Iowa State University, Ames, Iowa 50011, USA*

[3]*Institut Jean Lamour, UMR 7198 CNRS, Nancy-Université–UPV-Metz, École des Mines de Nancy, Parc de Saurupt, CS14234, F-54042 Nancy, France*

[4]*Institute of Physical Research & Technology, Department of Physics & Astronomy, Iowa State University, Ames, Iowa 50011, USA*

[5]*Department of Mathematics, Ames Laboratory, U.S. Department of Energy, Iowa State University, Ames, Iowa 50011, USA*

(Received 2 June 2010; revised manuscript received 19 November 2010; published 9 December 2010)

Growth of Ag thin films on the twofold surface of a decagonal Al-Cu-Co quasicrystal is characterized by scanning tunneling microscopy, at different temperatures, and for coverages ranging from submonolayer to 11 monolayers. From prior work, three types of clean surface terraces are known to exist. By correlation with a bulk structural model, the major difference between them lies in their transition-metal (TM) content, two being aluminum-rich (0 and 15 at. % TM) and one being TM-rich (40–50 at. % TM). The present article focuses on understanding the difference between Ag film morphologies on these terminations, in terms of their chemical content. Growth is found to be smoother on the TM-rich terraces and rougher on the Al-rich ones. The first Ag atomic layer is even pseudomorphic on the TM-rich terraces. Roughness variation with temperature shows that the equilibrium morphology is two dimensional for TM-rich terraces and three dimensional for Al-rich terraces. The explanation of different growth modes in terms of different terrace compositions is supported by calculations of the adhesion energy of a Ag slab with Ag, Al, Cu, and Co slabs, using density-functional theory. For the Al-rich terraces, the roughness variation with temperature also indicates reentrant growth, i.e., anomalously smooth growth at low temperature due to kinetic effects.

DOI: 10.1103/PhysRevB.82.224204 PACS number(s): 61.44.Br, 68.37.Ef, 68.55.A−, 71.15.Mb

I. INTRODUCTION

Quasicrystals are fascinating materials because they are quasiperiodic but, in some cases, they are as well ordered as the best conventional single crystals.[1] This structural order is usually associated with "forbidden" rotational symmetries, such as fivefold, tenfold, or 12-fold. Decagonal (tenfold) phases are periodic (P) in one of the three dimensions. This structural feature provides a great opportunity to compare the effect of quasiperiodicity and periodicity on their properties within a single sample, specifically because both periodic and quasiperiodic axes are captured (and are perpendicular) in a twofold plane.[2] For this reason, some groups chose decagonal phases for investigations of thermal and electrical conductivity and discovered that transport is much different along periodic and quasiperiodic directions.[3–5] A decagonal phase was also chosen by Park *et al.*,[6,7] who studied the friction coefficient of the twofold surface of a decagonal Al-Ni-Co quasicrystal at the atomic scale, using an atomic force microscope in ultrahigh vacuum. They found that the friction coefficient was also strongly anisotropic, being eight times lower in the quasiperiodic direction. This was attributed to lower energy dissipation due to either the electronic or phononic structure or both.

In order to understand the properties of quasicrystalline surfaces further in terms of their atomic structure, modeling is needed. However, modeling is difficult in such complex systems. One problem is the chemical complexity, to our knowledge, all stable decagonal phases are ternary or higher. A way to circumvent this would be to grow, measure, and model the properties of a single component, pseudomorphic thin film. To this end, successful and unsuccessful attempts have been made over the past decade with films of different single elements, such as Ag, Pb, Cu, Bi, and Na, on different quasicrystalline surfaces.[8–13] Pseudomorphic Ag islands have been observed by scanning tunneling microscope (STM) on the fivefold Al-Pd-Mn quasicrystalline substrate in the submonolayer range.[14] However, above submonolayer coverage, three-dimensional (3D) islands develop exhibiting quantum size effects.[14–16] On GaAs(110), Ag films show one-dimensional quasiperiodic modulation leading to a complex electronic band structure along the quasiperiodic direction observed by angle-resolved photoemission spectroscopy.[17] Films have rarely been prepared on twofold surfaces[8] even though such a system could be used to test whether the anisotropic friction coefficient is transmitted to the pseudomorphic single-element thin film.

In the present work we describe a step toward that goal, namely, the characterization of Ag thin films grown on the twofold surface of the decagonal (d-)Al-Cu-Co quasicrystal. In a recent paper, we elucidated the atomic structure of the surface by comparing experimental low-energy electron diffraction and STM data[18] with a structural model derived from a five-dimensional Patterson analysis of x-ray diffraction data from Deloudi *et al.*[19] Three surface terminations were found to exist, based on different structures present on different terraces. From the bulk model, the surface atomic density of the selected terminations is close to that of Al(111) and the compositions range from 50–60 at. % Al to pure Al. Taking advantage of this previous characterization, we will

show that different kinds of terraces support distinctly different growth modes of Ag films, attributable to their different compositions. This explanation is supported by density-functional theory (DFT) calculations of the adhesion energy of Ag with each of the pure elements that constitute the quasicrystalline substrate. Kinetic vs thermodynamic effects are also elucidated by experiments at different temperatures.

II. DETAILS OF EXPERIMENTS AND CALCULATIONS

The surface investigated is normal to a twofold [10000] direction, using the same notation as Duguet *et al.*[18] The sample has a bulk one-dimensional periodicity of 0.84 nm, two times the basic 0.42 nm periodicity of decagonal phases. This is observed in selected area electron-diffraction patterns along $[001\bar{1}0]$ showing diffuse interlayer lines that reflect the 0.84 nm superstructure.[20]

Experiments are performed in an ultrahigh-vacuum chamber equipped with an Omicron variable temperature (VT)-STM and a scanning auger microscope and with a base pressure in the low 10^{-11} mbar range. Surface preparation consists of repeated sputtering (Ar^+, 2 keV) and annealing (from 973 to 1073 K) cycles. Auger is used periodically to check surface cleanliness. Ag deposition at different temperatures is carried out using an e-beam evaporator facing the STM stage at a working pressure below 2×10^{-10} mbar. For submonolayer deposition on this quasicrystal, one cannot readily identify the fraction of the surface covered by Ag. Thus, the flux rate of 0.4 ML/min for our deposition source was determined from the STM images of well-defined two-dimensional (2D) islands with known local coverage formed during submonolayer deposition on other substrates, where we used the same deposition source and settings. Coverage is calculated as the product of flux and time and is reported in units of ML, where ML is defined as the fractional area covered by Ag.

The annealing temperature is monitored with an optical pyrometer (emissivity set to $\varepsilon=0.35$). Calibration of the pyrometer is performed with a thermocouple attached to the sample holder. The STM images are analyzed with WSXM software.[21] Additional details about crystal growth and surface preparation can be found elsewhere.[18,20]

Benchmark DFT calculations are performed using the plane-wave-based Vienna *ab initio* simulation package (VASP) to assess the adhesion of an fcc slab of Ag to fcc slabs of different metal substrates (Al, Cu, Co, and Ag). The details of our DFT calculations (e.g., use of the Perdew-Burke-Ernzerhof form of the generalized gradient approximation and of the projector augmented wave approach to describe electron-ion interactions) are similar to our previous calculations for Ag films and have been described in detail previously.[22] For the present work, the **k** mesh is chosen as $20\times20\times1$ for supported or unsupported Ag(110) films and $30\times30\times1$ for supported or unsupported Ag(100) or Ag(111) films (the latter systems demanding a finer mesh for convergence[22]). Results for adhesion are reported choosing all slab thicknesses to be four layers (e.g., a total of eight layers for the substrate/overlayer system). Tests taking thicker five layer slabs reveal relatively small variations in the adhesion energies (±0.05 eV/site) due to quantum size effects,[22] so we conclude that the four layer results are reliable. In order to match lattices of different metals in these analyses, we always use a 2D lateral lattice constant of 0.4166 nm, corresponding to the DFT value for bulk fcc Ag (i.e., the Cu, Co, or Al slabs are strained to match Ag, at the interface). Also, since the cohesive energy of bulk fcc Co is very close to that of bulk hcp Co,[23] we force a fcc structure for the Co slab. Magnetism has also been taken into account in Co-related calculations. The Ag *overlayer* is always relaxed in the direction orthogonal to the interface (vertically). Finally, we perform two types of calculations for all Ag on-substrate systems: one type with the substrate fixed to the bulk Ag lattice constant (in the three directions) and another with the substrate relaxed vertically (but with the lateral unit cell still fixed to match that of the appropriate face of Ag).

III. EXPERIMENTAL RESULTS

A. Clean surface

The twofold surface of the d-Al-Cu-Co quasicrystal is described in detail in Ref. 14. This section is a brief review. Figure 1 summarizes the main structural features of the surface. It also shows a surface region [Fig. 1(a)] that is monitored during a set of consecutive Ag depositions, as described in Sec. III B.

Three types of terraces occur at the surface. The three model terminations corresponding to the three types of terraces are shown in Fig. 1(e). The following notations will be used for the *model* terminations: (i) the first two types are pure and almost pure, Al. We call them 100%-Al and 85%-Al, where the numbers give the atomic per cents. The density of the 0.11-nm-thick surface layers is 10 atoms/nm^2. (ii) The third type is richer in the transition metals (TM), containing 40–50 at. % Co and Cu. That type of terrace will be called TM-rich. The density of the 0.11-nm-thick surface layers is 11 atoms/nm^2.

Experimentally, we distinguish the three types of terraces by looking at their atomic arrangements compared to the model termination and image bias dependence. The most striking difference occurs between the TM-rich terraces and the two others.

Unlike the Al-rich ones, images of the TM-rich terraces are strongly bias dependent. This is shown in Figs. 1(b) and 1(c), where the same region of a TM-rich terrace is scanned under opposite biases. The difference between the two images is attributed to the strong variation in electronic density in the vicinity of the Fermi level for the transition metals. On the TM-rich model termination [Fig. 1(e)], one can see that pure TM atomic lines alternate with pure Al atomic lines in the aperiodic (A) direction but it is only the TM lines that are responsible for the bias dependence. Note that the periodicity of all the rows is 0.84 nm, different than the bulk model. Also, in Fig. 1(c), darker regions are nanodomains within the TM-rich terraces whose contrast is less dependent on the bias [see Figs. 1(b) and 1(c)]. This suggests that these nanodomains are Al-rich, rather than TM-rich.

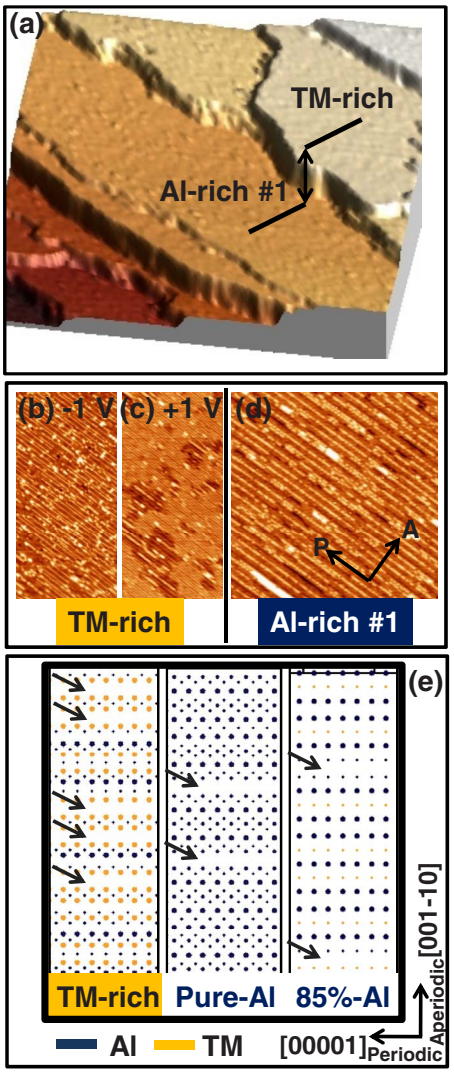

FIG. 1. (Color online) Summary of structural features observed on the clean twofold d-Al-Cu-Co surface. (a) Step terrace morphology (1000×1000 nm^2). Panels (b) and (c) show a small region (100×48 nm^2) of the TM-rich terrace in (a), imaged at different tip biases. Panel (d) shows a 100×100 nm^2 STM images of the Al-rich #1 terrace. (b), (c), and (d) orientation corresponds to the aperiodic (A) and periodic (P) axes shown in (d). STM images were recorded at 0.5 nA tunneling current. Panel (e) shows the three 10×3 nm^2 corresponding model terminations. Blue (dark) dots represent Al atoms and orange (bright) dots represent TM atoms. The size of the dots is a function of their vertical position (larger size is closer to vacuum). Arrows indicate 0.3-nm-wide line separations that are called "low-density rows" in the text.

Both Al-rich types of terrace are found at the surface but it has been difficult to assign a model termination unambiguously[18] because their compositions and densities are very close, according to the bulk model. Elsewhere, we will present distinct evidence that the Al-rich #1 terraces can be assigned as the 85%-Al termination and the Al-rich #2 terraces as the 100%-Al termination.[24]

Experimentally, the existence of two different types of Al-rich terraces is revealed by their defects, which are defined as *local* features that do not correspond to the model terminations. Namely, defects here refer to troughs, adrows, and different periodicity in certain rows than the rest of the terrace. By overlaying the model terminations on the experimental data, we determined[18] that the defects are always located along rows of low atomic density in the model [shown by arrows in Fig. 1(e)], running in the periodic direction. On Al-rich #1 terraces, the defects are adrows and a few troughs at 300 K [see Fig. $5c_1$], and exclusively troughs above 300 K [see Fig. $5c_3$]. Presumably, the adrows disappear due to increased adatom mobility with temperature. The Al-rich #2 terraces exhibit stripes in STM that consist of a doubling of the periodicity (0.84 nm), compared to the rest of the terrace (0.42 nm), along the low-density rows in the bulk model [see arrows, Fig. $5b_1$]. In the prior analysis of the clean surface, this was attributed to a mechanism in which atoms rearrange from their bulk positions to circumvent the formation of low-density rows.

B. Growth at 300 K

STM is performed on the TM-rich and Al-rich #1 terraces shown in Fig. 1(a), after consecutive Ag depositions at 300 K. Coverages are 0.5, 1.0, 1.5, 3, 5, 8, and 10 ML. We will show that growth is different on the two terraces by comparing roughness measurements and growth morphologies.

Figure 2 shows the STM results for a selection of coverages. Many other experiments were done to check the reproducibility of the results. At 0.5 ML, the TM-rich terrace shows regions that exhibit two different Ag growth modes, as seen in Fig. 2(a). We attribute this to the existence of nanodomains within the terrace, discussed in Sec. III A. Based on comparison with growth morphology on the Al-rich terraces (below), the regions that have a striped appearance are the nanodomains, and the smooth-looking regions are the TM-rich regions. On the TM-rich regions, the terrace is covered smoothly by Ag at this coverage. One piece of evidence for this is that the STM contrast is no longer bias dependent. Further proof will be given in Sec. III D.

From Fig. 2, for any given coverage of Ag, it can be seen that the root mean-square (rms) roughness is lower on the TM-rich terrace than on the Al-rich #1 terrace. On the former they would be even lower if not averaged with the rougher nanodomain areas. This indicates that growth is smoother on TM-rich terraces than on Al-rich terraces.

On the Al-rich #1 terrace, Ag grows in the form of long rows, or stripes, in the periodic direction, enhancing features that are present already on the clean surface. Before Ag deposition, the extant rows are 0.06 to 0.10 nm high, relative to the lowest plane in the image. After 0.5 ML deposition [see Fig. 2(e)] they have grown to 0.15 to 0.22 nm high. Since the region between the stripes is not obviously modified and the height of the stripes increases, it is likely that Ag grows only on top of the stripes (at coverage up to 0.5 ML). At higher coverage, the stripes also grow laterally and at 10 ML the higher layers coalesce laterally, hence reducing the spatial anisotropy. At 10 ML, black holes in Fig. 2(h) are 1.6 nm (roughly eight layers) deep, suggesting that the holes reach down to or nearly to the clean surface.

On the TM-rich terrace, there is still a tendency for the formation of Ag islands that are elongated in the periodic

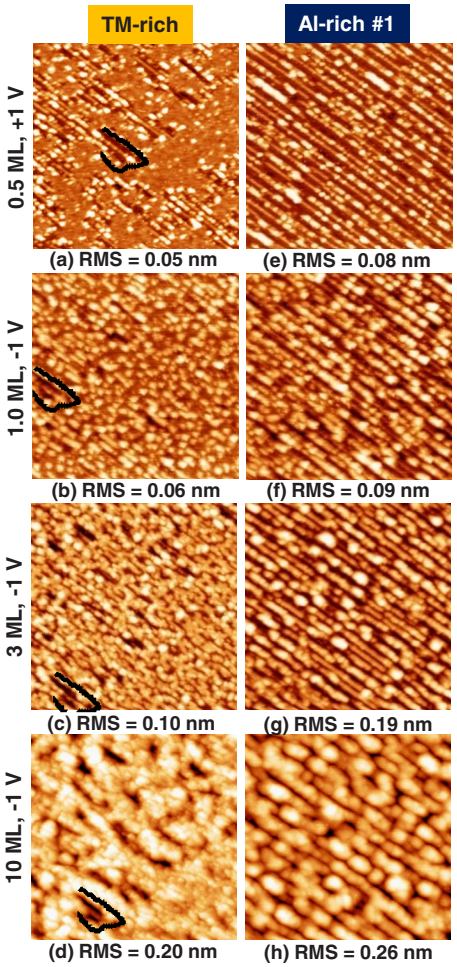

FIG. 2. (Color online) STM images of the TM-rich and Al-rich #1 terraces shown in Fig. 1(a), after consecutive depositions of Ag at 300 K. All images are 100×100 nm^2 and are recorded with a tunneling current of 0.5 nA. Coverage and tip bias are given for each row on the left. rms roughness are given below each image. The roughness measurements were performed after low-noise filtering, using the WSXM software. Black line drawn in the left column images limits a nanodomain on the TM-rich terrace. A tip effect increases the apparent thickness of features in (b).

direction. At 1.0 ML, we observe the formation of small islands on top of the smooth Ag layer [see center of Fig. 2(b)] At higher coverage, coalescence of the Ag islands tends to form a film that is smoother and more isotropic than on the Al-rich #1 terrace.

C. Growth of Ag thin films at higher temperature

Figure 3 shows STM images of the TM-rich and Al-rich #1 terraces after deposition at 365 K and after annealing to 420 K, at the fixed coverage of 5 ML. Other experiments show that the result of annealing to 420 K is quite similar to deposition at 420 K. The temperature dependence exhibited at this coverage, 5 ML, is similar to that at coverages of 0.5, 1.5, and 3 ML.

As at 300 K, Ag grown at 365 K is smoother on the TM-rich terrace than on the Al-rich terrace. Specifically, the

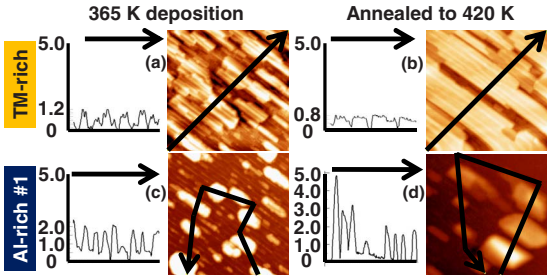

FIG. 3. (Color online) STM images (100×100 nm^2) of 5 ML Ag on a TM-rich and an Al-rich #1 terrace, deposited at 365 K and annealed to 420 K and held at 420 K during scanning. Each line profile corresponds to the path indicated by the arrow within the STM image to its right. The tunneling current is 0.5 nA for all images and bias voltage is +1 V in (a), +1.5 V in (b), and −1 V in [(c) and (d)].

island heights on the TM-rich terrace range from 0.2 to 1.0 nm and from 0.4 to 2.0 nm on the Al-rich terrace. Consequently, the area covered by the islands is higher on the TM-rich than on the Al-rich terraces, an effect which can be seen directly in Fig. 3(a) vs Fig. 3(c). The difference in roughness is strongly accentuated by annealing the Ag thin film to 420 K: the TM-rich terrace gets still smoother (0.4–0.8 nm high islands) whereas the Al-rich terrace gets still rougher (up to 5.0 nm high islands). The trend is summarized in Fig. 4, which shows the rms roughness of surface features as a function of temperature for 5 ML Ag films. At all temperatures measured, 300–420 K, the roughness is higher on the Al-rich terrace than on the TM-rich terrace.

The data in Fig. 4 show another noteworthy feature: the shape of the curve depends on the chemical composition of the termination. On the Al-rich terrace, the film becomes continuously rougher from 300 to 420 K, whereas on the TM-rich terrace, the film becomes first rougher, then smoother, roughness passes through a maximum. One can safely assume that the trend at the highest temperature reflects an approach to equilibrium whereas at lowest tempera-

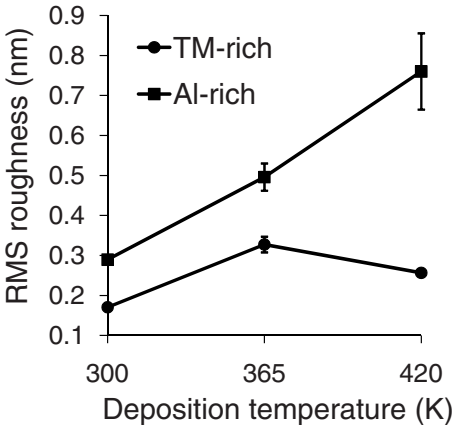

FIG. 4. rms roughness as a function of deposition temperature (except for Al-rich at 420 K, where the film is annealed to 420 K after deposition at 365 K). Roughness is obtained from images of size 100×100 nm^2. Error bars correspond to standard deviations and are sometimes smaller than the data marker.

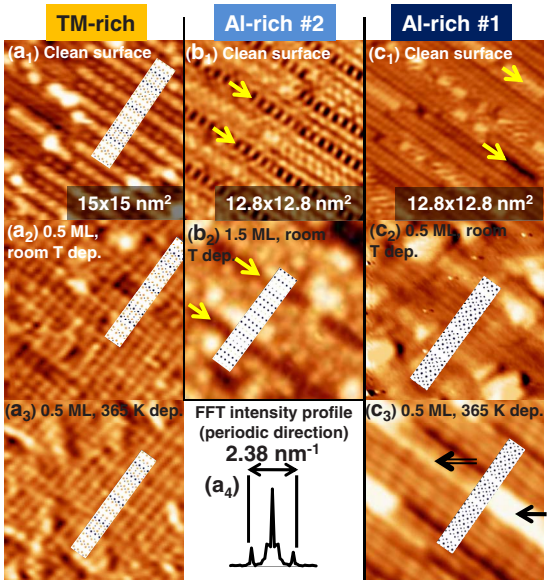

FIG. 5. (Color online) Clean surface terraces and 0.5 ML Ag films deposited at 300 K and at 365 K on (a) a TM-rich terrace and (c) an Al-rich #1 terrace. Panel (b) shows 1.5 ML deposited at 300 K on an Al-rich #2 terrace. Corresponding model terminations are superimposed for a better understanding of the surface features. All the STM images except the clean surface ones are 14.5 $\times$ 14.5 nm^2 and were recorded at -1 V and 0.5 nA. A smooth FFT filtering has been applied to the STM images in (a) and added to the same duplicate image in derivative mode. Arrows show what are referred in the text as doubled periodicity rows in panel (b) and adrows and troughs in panel (c_1). The single-line arrow in panel (c_3) shows an elongated island and the double-line arrow shows a bright stripe covering a trough.

ture it may be strongly influenced by kinetics. Therefore, we conclude that the equilibrium morphology of Ag on the Al-rich terrace is rough (more 3D) but on the TM-rich terrace it is smooth (more 2D). Furthermore, at 300 K, the *kinetics* of film growth on the TM-rich terrace apparently contributes to a metastable morphology which is *smoother* than it would be otherwise at this relatively low temperature. As some of the kinetic limitations are removed, i.e., in going from 300 to 365 K, the film becomes rougher. A possible explanation is given in Sec. V.

D. Detailed structure of Ag films at low coverage

Figure 5 shows the structures, at high magnification, of all three types of terraces both with and without Ag. (We did not show data for Al-rich #2 terraces previously because Ag growth was not monitored systematically on that kind of terrace.) Figure 5(a) shows the uncovered and 0.5 ML Ag covered, TM-rich terrace. Ag is deposited at 300 K [Fig. $5a_2$] and 365 K [Fig. $5a_3$]. The images for the two different deposition temperatures are similar. At 300 K, Ag forms a smooth layer. This is shown by comparing the clean TM-rich terraces with the ones after deposition [Fig. $5a_1$ vs Figs. $5a_2$ and $5a_3$]. From the overlaid model termination (white insets) one can see that the brightest features are the mixed rows of Al-TM atoms. Their contrast remains unaffected after deposition. In between these rows lie the pure rows of TM atoms and they are affected when Ag is present. Since contrast difference between rows on TM-rich terraces is an electronic effect and supposedly not topographic and given the flatness of the Ag layer at 0.5 ML, we assume that the whole surface investigated in Figs. $5a_2$ and $5a_3$ is covered by Ag. Moreover, STM images are no longer bias dependent as they were before deposition. In the periodic direction [as defined in Fig. 1(d)], fast Fourier transforms of the STM images show a periodicity that corresponds to $(2.38/2)^{-1} \approx 8.4$ nm [Fig. $5a_4$], the same as the periodicity of the TM-rich terraces. Altogether, this indicates that Ag is pseudomorphic at a coverage of 0.5 ML, on the TM-rich terraces.

Figure 5(c) shows STM images of the same coverage of Ag at 300 K [Fig. $5c_2$] and 365 K [Fig. $5c_3$] on a terrace of the Al-rich #1 type. The terrace before deposition is shown for reference in Fig. $5c_1$. The low-density rows in the model [see arrows in Fig. 1(e)] are associated with black troughs in the image [see lower arrow in Fig. $5c_1$]. Ag forms elongated islands centered in between these low-density rows.

This is observed more easily after the higher temperature deposition in Fig. $5c_3$, where an example of an elongated island is indicated by the single-line arrow. It is connected to another bright elongated Ag island by a bright stripe covering a trough, indicated by the double-line arrow. Such troughs are presumably unfavorable and their occurrence seems to be circumvented by Ag trapping and growth. We therefore propose that Ag islands are formed following a two-step mechanism, at 365 K. Ag first fills the troughs giving rise to a Ag stripe. Then, the stripe extends laterally until it covers the region between two stripes, leading to the formation of a Ag island centered between two troughs (or low-density rows).

At 300 K, troughs are almost totally replaced by adrows of intrinsic atoms, before deposition. Hence, Ag deposition reflects only the second step of the mechanism proposed above. Troughs are already filled. Then Ag covers the region between two adrows to form Ag islands centered between low-density rows of the model [Fig. $5c_2$]. Height of the Ag rows is 0.1 ± 0.02 nm. Between the Ag islands, no difference is found in atomic arrangement when compared to the clean surface at both temperatures.

Figure 5(b) shows STM images of a clean Al-rich #2 terrace, and another Al-rich #2 terrace with 1.5 ML Ag. As noted in Sec. III A, the terraces exhibit a defect in the form of a doubled periodicity [see arrows in Fig. 5(b)] along the low-density rows of the model termination. Along those specific atomic rows the periodicity is 0.84 nm whereas the rest of the terrace shows a 0.42 nm periodicity. Surprisingly, after deposition of 1.5 ML of Ag at 300 K, the 0.84 nm lines are still visible, although more diffuse. Ag does not cover the reconstruction but grows in between it.

IV. ADHESION ENERGY CALCULATIONS

One simple way of determining thermodynamic growth mode in A on B heteroepitaxy is to use the Bauer criterion.[25,26] For this study, the most convenient form of that criterion is

TABLE I. Adhesion energy (in units of electron volt per unit cell) of the Ag/Ag, Ag/Al, Ag/Cu, and Ag/Co systems, calculated by using DFT. Results are presented for fcc low-index planes (110), (111), and (100) and for fixed and relaxed substrates, in which the Ag overlayer is always relaxed.

	β_{AB}		
System	(110)	(111)	(100)
Ag/Ag (fixed)	2.78	1.36	1.76
Ag/Ag (relaxed)	2.70	1.36	1.76
Ag/Al (fixed)	1.51	0.83	1.05
Ag/Al (relaxed)	1.51	0.83	1.06
Ag/Cu (fixed)	1.93	0.98	1.27
Ag/Cu (relaxed)	1.47	0.91	1.19
Ag/Co (fixed)	2.20	1.13	1.46
Ag/Co (relaxed)	1.36	0.99	1.34

$$\beta_{AB} < 2\sigma_A \rightarrow 3D \text{ growth } \beta_{AB} > 2\sigma_A \rightarrow 2D \text{ growth},$$

where σ_A is the surface energy for material A and β_{AB} is the adhesion energy of A to B. β_{AB} is defined as "the work gained per surface area when putting into contact a crystal A with a crystal B in epitaxial orientation in such a way that the interface reaches its equilibrium."[27] Thus, the adhesion energy of A to A satisfies $\beta_{AA}=2\sigma_A$ and the above criterion amounts to a direct comparison of two adhesion energies. In principle, β_{AB} (and β_{AA}) can be determined from DFT analysis by theoretically approaching an overlayer slab of metal A and a substrate slab of metal B (metal A) with the same orientation.

In this work, we perform DFT calculations on simplified interfaces (as described in Sec. II) to test the idea that different chemical compositions on the terraces may promote different growth modes of Ag. Using DFT, we calculate the adhesion energy of a fcc Ag overlayer with itself as a substrate and with a substrate slab of each of the three elements that comprises the quasicrystal: Al, Cu, and Co. From the trend in the calculated adhesion energies, we can provide insight into the observed Ag morphologies on different types of terraces on the alloy substrate (a much more complex system).

The basic idea is to determine the energies (E_A and E_B) per lateral unit cell of two separate slabs of element A and element B, then put A and B into contact—creating an A/B interface—and calculate the total energy per lateral unit cell of the new system (E). The interface adhesion energy per unit site is then determined from

$$\beta_{AB} = E_A + E_B - E.$$

Table I shows the calculated adhesion energies for the Ag/Ag, Ag/Al, Ag/Cu, and Ag/Co, overlayer/substrate systems. Calculations have been performed for the fcc low-index planes (110), (111), and (100) and for fixed and relaxed substrates. For the latter, the slabs are relaxed both when separated and after creation of the A/B system interface. This treatment is appropriate for consistent calculation of adhesion energies.

The most pertinent observation from this analysis comes from comparison of results for the Ag/TM and Ag/Al systems: the general trend (with one exception discussed in the next paragraph) is that adhesion of Ag overlayer to the TM substrates is stronger than to the Al one. However, adhesion of Ag to Ag slabs is even stronger. This indicates that the driving force for rough growth is stronger on the Al slab than on the TM slab but in neither case should the equilibrated Ag film be smooth. Superficially, this contradicts the conclusion from the experimental data, that equilibrated Ag films on the TM-rich terraces of the quasicrystal would be 2D. However, our pure fcc TM and Al slabs provide very simplistic models for the chemically and structurally complex terraces of the alloy substrate. The main point is that DFT corroborates and explains the experimental trend in roughness of the Ag films with chemical composition of the terraces.

Interestingly, the above analysis indicates that adhesion of Ag to the TM slab is significantly enhanced when the interlayer spacing in the TM substrate is forced to that of Ag rather than relaxed. Presumably, relaxation facilitates enhanced TM-TM binding and reduced TM-Ag binding. [There is a large interlayer relaxation of TM atoms for a (110) plane with lateral unit cell fixed to that of Ag. This appears to create an artificially structured TM slab with anomalously weak adhesion to Ag. Thus, we discount this case when comparing adhesion of Ag to Al vs TM substrates.] In the experimental system, the TM atoms are probably fixed at or close to positions determined by the quasicrystal structure and thus their separations are even further removed from their bulk fcc values. Plausibly, this feature enhances adhesion to the quasicrystalline TM-rich terraces.

V. DISCUSSION

A. 2D vs 3D growth

The main observation regarding growth of Ag films on the (10000) surface of the d-Al-Cu-Co quasicrystal concerns the two different morphologies observed on the TM-rich and Al-rich terraces. At temperatures from 300 to 420 K, the Ag film is consistently smoother on the TM-rich terraces than on the Al-rich terraces. Furthermore, at the high end of our temperature range, Ag films on the TM-rich terraces become smoother as temperature increases while on the Al-rich terraces the films become rougher. This indicates that the difference in Ag morphology between the two types of terraces is due to thermodynamics, rather than kinetics. The latter feature indicates that the thermodynamic or equilibrium film structures correspond to smooth 2D films on TM-rich terraces and rough 3D films on Al-rich terraces. Behavior for deposition at lower temperature reflects kinetic limitations inhibiting equilibration. The presence of an Ehrlich-Schwoebel (ES) barrier inhibiting interlayer transport[28,29] would induce kinetic roughening of films with smooth equilibrium structures and kinetic smoothening of films with rough equilibrium structures.

In rationalizing our result for equilibrium film structures, it should be noted that a very simple rule-of-thumb is that, in equilibrium and in the absence of intermixing, the morphology of a film is 2D (at least in the first monolayer) if the film has a lower melting point than the substrate and 3D if the order of melting points is reversed. This simple rule is essentially based on the surface energies of A and B and ignores the effect of strain, relaxation at the interface, and the strength of chemical bonding between the two elements but nonetheless it holds true with surprising regularity. From this alone, one expects that Ag growth on Al will be 3D, whereas Ag growth on Cu or Co will be 2D. This is exactly what we observe on the QC surface. The validity of ascribing the difference in growth to chemical composition is further supported by a more sophisticated approach, i.e., our DFT calculations of the adhesion energies at simplified interfaces, which indicate a much stronger Ag-TM interaction than Ag-Al interaction. Finally, the data can be compared with experimental STM observations in simpler A on B systems. From those studies, Ag film morphology is 2D on Cu(111) (Ref. 30) and Cu(100) (Ref. 31) but 3D on Al(111).[32] There is evidence of alloying at very low Ag coverage on the latter two surfaces but overall the results are consistent with the DFT calculations and also with the simple rule-of-thumb.

B. Reentrant growth

For Ag films on the TM-rich terraces, roughness passes through a maximum between 300 and 420 K. This is reminiscent of the reentrant growth phenomenon in homoepitaxy.[33] In homoepitaxy, the equilibrium surface morphology is unequivocally smooth, so to a first approximation one expects that increasing temperature should simply lead to smoother films (up to the surface-roughening transition, which is always far higher than experimental temperatures). Instead of a smooth decrease in roughness vs growth temperature, the signature of reentrant growth in homoepitaxy is a *maximum* in roughness vs growth temperature. This has been reported for homoepitaxy on Pt(111),[34] Rh(111),[35] Ag(100),[36,37] and Cu(100).[38] The unexpected feature is the formation of smooth films at low temperature. Although a slightly different model has been put forward to explain each system, all explanations share two basic features. First, if an atom happens to land in an upper layer, the ES barrier inhibits it from moving into an empty spot in a lower layer. The second feature is that a characteristic lateral dimension of the metal islands is smaller at low temperature and that this smaller dimension facilitates either thermally activated or athermal movement of atoms into lower layers at low temperature. As temperature increases, the lateral dimension increases, leading to rougher films. Eventually temperature becomes high enough that the ES barrier is overcome, leading to smoother films again and hence the observed maximum in roughness.

The feature that distinguishes the proposed models is the mechanism of downward transport at low temperature. One mechanism, for which good evidence exists at least in the Ag/Ag(100) and Cu/Cu(100) systems, is downward funneling.[39,40] In this case, an atom that lands near a step edge "funnels downward" to an adsorption site in a lower layer. The feature that adsorption sites are fourfold-hollow sites rather than on-top sites also facilitates smoother growth in the absence of terrace diffusion.[41,42] It is conceivable that the very small Ag islands which form on TM-rich terraces at 300 K facilitate this downward funneling mechanism.

C. Anisotropic properties in a pseudomorphic film

An original objective was to see whether this would be a good system for testing anisotropic properties in pseudomorphic films. Unfortunately, that is not the case. Due to terrace heterogeneity, there is considerable heterogeneity in film structure across different terraces. The Ag film appears to be pseudomorphic on the TM-rich terraces, at least at submonolayer coverage. However, the situation is not clear on the Al-rich terraces, where 3D growth predominates.

VI. CONCLUSIONS

We have characterized growth of Ag thin films on the twofold surface of a decagonal Al-Cu-Co quasicrystal with scanning tunneling microscopy. Terraces of different chemical composition were identified from the presence of defects and from bias dependence in STM imaging. We focused the present paper on showing and explaining the difference between film morphologies on transition-metal-rich terraces (40–50 at. %) and aluminum-rich terraces. The Ag film was found to be smoother on the TM-rich terraces than on the Al-rich ones at all temperatures, 300 to 420 K. The difference was accentuated at the high end of the temperature range, suggesting that in equilibrium, Ag grows 2D on the TM-rich terraces and 3D on the Al-rich terraces. Additionally, we showed that the first Ag atomic layer is pseudomorphic on the TM-rich terraces. *Ab initio* calculations of the energy of adhesion of a Ag slab with either a Ag, an Al, a Cu, or a Co substrate supported the observed trend with chemical composition, i.e., Ag films smoother on the TM-rich terraces. On the TM-rich terraces, nanodomains were found at the surface as already described in the clean surface analysis.[18] On these nanodomains, Ag growth proceeds similarly to the Al-rich terraces.

ACKNOWLEDGMENTS

The experimental component of this work was partially supported by the Office of Science, Basic Energy Sciences, Materials Science Division of the U.S. Department of Energy (USDOE) under Contract No. DE–AC02–07CH11358 through the Ames laboratory. It was also partially supported by the European Network of Excellence on Complex Metallic Alloys (CMA) under Contracts No. NMP3-CT-2005-500145 and No. ANR-07-Blan-0270. The theoretical component of this work was supported by the National Science Foundation (NSF) through Grant No. CHE-0809472.

*Present address: Department of Chemical Engineering, Massachusetts Institute of Technology, Cambridge, MA 02139, USA.

[1] D. Shechtman, I. Blech, D. Gratias, and J. W. Cahn, Phys. Rev. Lett. **53**, 1951 (1984).
[2] J. Y. Park, D. F. Ogletree, M. Salmeron, R. A. Ribeiro, P. C. Canfield, C. J. Jenks, and P. A. Thiel, Phys. Rev. B **72**, 220201(R) (2005).
[3] J. A. Barrow, M. C. Lemieux, B. A. Cook, A. R. Ross, V. V. Tsukruk, P. C. Canfield, and D. J. Sordelet, J. Non-Cryst. Solids **334-335**, 312 (2004).
[4] P. A. Shields, M. Charlton, T. Lee, M. E. Zoorob, D. W. E. Allsopp, and W. N. Wang, IEEE J. Sel. Top. Quantum Electron. **15**, 1269 (2009).
[5] D.-l. Zhang, S.-c. Cao, Y.-p. Wang, L. Lu, X.-m. Wang, X. L. Ma, and K. H. Kuo, Phys. Rev. Lett. **66**, 2778 (1991).
[6] J. Y. Park, D. F. Ogletree, M. Salmeron, R. A. Ribeiro, P. C. Canfield, C. J. Jenks, and P. A. Thiel, Science **309**, 1354 (2005).
[7] J. Y. Park, D. F. Ogletree, M. Salmeron, R. A. Ribeiro, P. C. Canfield, C. J. Jenks, and P. A. Thiel, Phys. Rev. B **74**, 024203 (2006).
[8] V. Fournée, A. R. Ross, T. A. Lograsso, J. W. Evans, and P. A. Thiel, Surf. Sci. **537**, 5 (2003).
[9] V. Fournée and P. A. Thiel, J. Phys. D: Appl. Phys. **38**, R83 (2005).
[10] R. McGrath, J. A. Smerdon, H. R. Sharma, W. Theis, and J. Ledieu, J. Phys.: Condens. Matter **22**, 084022 (2010).
[11] H. R. Sharma, M. Shimoda, and A. P. Tsai, Adv. Phys. **56**, 403 (2007).
[12] J. A. Smerdon, H. R. Sharma, J. Ledieu, and R. McGrath, J. Phys.: Condens. Matter **20**, 314005 (2008).
[13] J. A. Smerdon, L. H. Wearing, J. K. Parle, L. Leung, H. R. Sharma, J. Ledieu, and R. McGrath, Philos. Mag. **88**, 2073 (2008).
[14] B. Ünal, V. Fournée, P. A. Thiel, and J. W. Evans, Phys. Rev. Lett. **102**, 196103 (2009).
[15] V. Fournée, H. R. Sharma, M. Shimoda, A. P. Tsai, B. Ünal, A. R. Ross, T. A. Lograsso, and P. A. Thiel, Phys. Rev. Lett. **95**, 155504 (2005).
[16] B. Ünal, V. Fournée, K. J. Schnitzenbaumer, C. Ghosh, C. J. Jenks, A. R. Ross, T. A. Lograsso, J. W. Evans, and P. A. Thiel, Phys. Rev. B **75**, 064205 (2007).
[17] P. Moras, W. Theis, L. Ferrari, S. Gardonio, J. Fujii, K. Horn, and C. Carbone, Phys. Rev. Lett. **96**, 156401 (2006).
[18] T. Duguet, B. Ünal, M. C. d. Weerd, J. Ledieu, R. A. Ribeiro, P. C. Canfield, S. Deloudi, W. Steurer, C. J. Jenks, J. M. Dubois, V. Fournée, and P. A. Thiel, Phys. Rev. B **80**, 024201 (2009).
[19] S. Deloudi, Ph.D. thesis, Eidgenössische Technische Hochschule, 2008.
[20] R. A. Ribeiro, S. L. Bud'ko, F. C. Laabs, M. J. Kramer, and P. C. Canfield, Philos. Mag. **84**, 1291 (2004).
[21] I. Horcas, R. Fernandez, J. M. Gomez-Rodriguez, J. Colchero, J. Gomez-Herrero, and A. M. Baro, Rev. Sci. Instrum. **78**, 013705 (2007).
[22] Y. Han and D.-J. Liu, Phys. Rev. B **80**, 155404 (2009).
[23] P. Thibaudeau and J. D. Gale, arXiv:0809.0198v1 (unpublished).
[24] T. Duguet, B. Ünal, J. Ledieu, J. M. Dubois, V. Fournée, and P. A. Thiel (unpublished).
[25] E. Bauer, F. Bonczek, H. Poppa, and G. Todd, Surf. Sci. **53**, 87 (1975).
[26] E. Bauer and J. H. Van Der Merwe, Phys. Rev. B **33**, 3657 (1986).
[27] *Current Topics in Materials Science*, edited by E. Kaldis (North-Holland, Amsterdam, 1979).
[28] G. Ehrlich and F. G. Hudda, J. Chem. Phys. **44**, 1039 (1966).
[29] R. L. Schwoebel and E. J. Shipsey, J. Appl. Phys. **37**, 3682 (1966).
[30] W. E. McMahon, E. S. Hirschorn, and T. C. Chiang, Surf. Sci. Lett. **279**, L231 (1992).
[31] P. T. Sprunger, E. Lægsgaard, and F. Besenbacher, Phys. Rev. B **54**, 8163 (1996).
[32] V. Fournée, J. Ledieu, T. Cai, and P. A. Thiel, Phys. Rev. B **67**, 155401 (2003).
[33] J. W. Evans, P. A. Thiel, and M. C. Bartelt, Surf. Sci. Rep. **61**, 1 (2006).
[34] R. Kunkel, B. Poelsema, L. K. Verheij, and G. Comsa, Phys. Rev. Lett. **65**, 733 (1990).
[35] F. Tsui, J. Wellman, C. Uher, and R. Clarke, Phys. Rev. Lett. **76**, 3164 (1996).
[36] K. J. Caspersen, C. R. Stoldt, A. R. Layson, M. C. Bartelt, P. A. Thiel, and J. W. Evans, Phys. Rev. B **63**, 085401 (2001).
[37] C. R. Stoldt, K. J. Caspersen, M. C. Bartelt, C. J. Jenks, J. W. Evans, and P. A. Thiel, Phys. Rev. Lett. **85**, 800 (2000).
[38] C. E. Botez, P. F. Miceli, and P. W. Stephens, Phys. Rev. B **64**, 125427 (2001).
[39] J. W. Evans, D. E. Sanders, P. A. Thiel, and A. E. DePristo, Phys. Rev. B **41**, 5410 (1990).
[40] H. C. Kang and J. W. Evans, Surf. Sci. **271**, 321 (1992).
[41] J. W. Evans, Phys. Rev. B **39**, 5655 (1989).
[42] D. K. Flynn, J. W. Evans, and P. A. Thiel, J. Vac. Sci. Technol. A **7**, 2162 (1989).